

# EFFECTS OF PARTICLE ENTRAINMENT ON HEAT TRANSFER PAST PARTICLES IN AN OSCILLATING FLOW

Man Yeong Ha\*

(Received September 9, 1991)

In order to investigate the effect of the particle entrainment on the heat transfer past particles entrained in an oscillating flow with and without a steady velocity, the two dimensional, unsteady, laminar conservation equations for mass, momentum and energy transport in the gas phase are solved numerically in spherical coordinates. The particle momentum equation is also solved simultaneously with the gas phase equations. The numerical solution gives the particle velocity variation as well as the gas phase velocity and temperature distribution as a function of time. The local and space-averaged Nusselt number with particle entrainment is compared with that without particle entrainment. In the case of an oscillating flow with a steady velocity, the values of the space-averaged Nusselt number with particle entrainment are lower than those without particle entrainment at frequencies of 50 and 2000 Hz since the moving particle is entrained in the steady velocity. In the case of an oscillating flow without a steady velocity, the space-averaged Nusselt number with entrainment at a frequency of 50 Hz is slightly lower than that without particle entrainment, with a phase lag. At 2000 Hz, the space-averaged Nusselt number with and without particle entrainment is almost the same, due to very small particle entrainment.

**Key Words:** Particle Entrainment, Heat Transfer, Oscillating Flow

## NOMENCLATURE

|            |  |
|------------|--|
| $dB$       | : Decibel                                    |
| $D$        | : Diameter                                   |
| $f$        | : Frequency                                  |
| $h_\theta$ | : Local heat transfer coefficient            |
| $i$        | : Static enthalpy                            |
| $k$        | : Thermal conductivity                       |
| $m_p$      | : Particle mass                              |
| $Nu$       | : Nusselt number                             |
| $P$        | : Pressure                                   |
| $Pr$       | : Prandtl number                             |
| $r$        | : Radial position                            |
| $R$        | : Radius of particle                         |
| $Re_0$     | : Steady Reynolds number ( $U_0 D / \mu$ )   |
| $Re_1$     | : Acoustic Reynolds number ( $U_1 D / \mu$ ) |
| $S$        | : Strouhal number ( $fD / U_1$ )             |
| $S_\phi$   | : Source term for general variable $\phi$    |
| $t$        | : Time                                       |
| $T$        | : Temperature                                |
| $T$        | : Period                                     |
| $u_r$      | : Radial velocity                            |
| $u_\theta$ | : Axial velocity                             |
| $U_0$      | : Steady slip velocity                       |
| $U_1$      | : Acoustic peak velocity                     |
| $v_g$      | : Gas velocity                               |
| $v_p$      | : Particle velocity                          |

Greek symbols

|                    |   |
|--------------------|---|
| $\beta$            | : Angular direction defined in the streamwise direction |
| $\Gamma_\phi$      | : Diffusivity for general variable $\phi$               |
| $\varepsilon_\phi$ | : Convergence criteria                                  |
| $\varepsilon$      | : Velocity ratio  |
| $\theta$           | : Angular direction                                     |
| $\mu$              | : Viscosity   |
| $\rho_g$           | : Gas density   |
| $\tau$             | : Dimensionless time ( $ft$ or $t/T$ )                  |
| $\tau_s$           | : Quasi-steady dimensionless time                       |
| $\phi$             | : General variable given in equation (1)                |
| $\omega$           | : Angular frequency                                     |
| $\infty$           | : Infinity  |

## Subscripts

|          |                       |
|----------|-----------------------|
| $g$      | : Gas                 |
| $new$    | : New values          |
| $old$    | : Old values          |
| $p$      | : Particle            |
| $r$      | : Radial              |
| $s$      | : Space-averaged      |
| $s$      | : Separation          |
| $0$      | : Steady              |
| $0$      | : Initial             |
| $1$      | : Acoustic            |
| $\theta$ | : Angular             |
| $\phi$   | : Dependent variables |
| $\infty$ | : Infinity            |

## 1. INTRODUCTION

The effect of an oscillating flow field with and without a

\*Department of Mechanical and Production Engineering, Research Institute of Mechanical Technology, Pusan National University, Kunjung Ku, Pusan, 609-735, Korea

steady velocity component on heat and mass transfer from single spherical particles and droplets has been a topic of investigation since the late 1930s (Marthelli and Boelter, 1939). Some examples of these theoretical and experimental studies can be found in the previous works (Baxi and Ramachandran, 1969, Mori et al., 1969, Gibert and Angelino, 1974, Larsen and Jensen, 1978, Rawson, 1988). These publications report an increase, decrease or unnoticeable change in heat and mass transfer, depending on the frequency and the magnitude of the steady and oscillating flow. Zinn et al. (1982) and Faeser (1984) indicated the positive effects of high intensity acoustics on coal combustion by using acoustic drivers or pulsed combustion. Koopmann et al. (1989) investigated the effects of high intensity acoustic fields on the rate of combustion of coal-water slurry fuel in the sonic combustor. Yavuzkurt et al. (1989) and Yavuzkurt and Ha (1989) calculated a decrease of 15.7% and 12.1%, respectively, in the char burn-out length for a sound pressure level of 160 dB and at a frequency of 2000 Hz compared to the case with no sound for the combustion of 100 $\mu$ m pulverized coal or coal water slurry fuels.

The previous studies are generally concentrated on experimental and theoretical studies showing the effects of oscillating flow field on heat and mass transfer and combustion past particles, in which it is usually assumed that the particle is stationary relative to its gaseous environment. Thus, the particle momentum equation is not included with the constant slip velocity between the particle and the bulk gas stream. However, in the initial stages of combustion of pulverized coal or coal-water slurry droplets, there exists a steady slip velocity,  $U_b$ . This steady slip velocity decreases during combustion since coal particles or particle agglomerates become entrained in the main gas flow. During the later stages of pulverized coal or coal-water slurry fuel combustion, the slip velocity between the entrained particles and the gas is quite low for a significant period of time, leading to low heat and mass transfer to and from the particles. For this situation, the particle momentum equation should be solved simultaneously with gas phase equations and the slip velocity continuously changes depending on the particle trajectories.

As can be seen, the previous experimental and theoretical studies concentrate on heat transfer past stationary particles in an oscillating flow with a steady velocity. There are little detailed studies showing the effects of particle entrainment on heat transfer past particles in an oscillating flow. The objective of the present study is to fill out this gap and to investigate heat transfer past particles entrained in an oscillating flow with a steady velocity component. In order to achieve this objective, an oscillating flow,  $U_1 \cos 2\pi ft$ , induced by the high intensity acoustic fields is superposed on the mean steady flow,  $U_b$ , in the present study. The two dimensional, unsteady conservation of mass, momentum and energy equations for a laminar flow past particles in spherical coordinates was solved simultaneously with the particle momentum equation. The results obtained considering particle entrainment are compared with those without entrainment.

## 2. GOVERNING EQUATIONS AND BOUNDARY CONDITIONS

The hydrodynamic and thermal characteristics of an oscillating flow created by an acoustic field over a single particle are studied by solving the unsteady and two dimensional

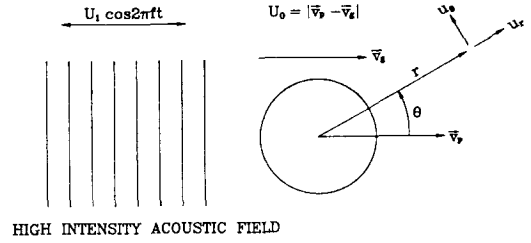


Fig. 1 Schematic diagram showing the geometry and some of the nomenclature used to simulate heat transfer past a spherical particle entrained in an oscillating flow

axisymmetric conservation equations for constant property, laminar flow with the following common form (see Patankar, 1980) :

$$\begin{aligned} \frac{\partial}{\partial t}(\rho\phi) + \frac{1}{r^2} \frac{\partial}{\partial r}(r^2 \rho u_r \phi) + \frac{1}{r \sin \theta} \frac{\partial}{\partial \theta}(\sin \theta \rho u_\theta \phi) \\ = \frac{1}{r^2} \frac{\partial}{\partial r}(\Gamma_\phi r^2 \frac{\partial \phi}{\partial r}) + \frac{1}{r^2 \sin \theta} \frac{\partial}{\partial \theta}(\Gamma_\phi \sin \theta \frac{\partial \phi}{\partial \theta}) + S_\phi \quad (1) \end{aligned}$$

The flow field and the particle geometry with some nomenclature are shown in Fig. 1. In the conservation of momentum equation,  $\phi = u_r, u_\theta$  represents the velocities in the radial  $r$  and axial  $\theta$  directions, respectively. In the energy equation  $\phi = i$  is the static enthalpy. The source terms  $S_\phi$  in Eq. (1) are given in Table 1. The quantities are allowed to vary in the radial ( $r$ ) and axial ( $\theta$ ) directions whereas a circumferential symmetry is assumed around an axis which passes through the center of the particle and is parallel to the flow direction.

The governing Eq. (1) has the following initial and boundary conditions :

Initial Conditions ( $t=0$ ) :

$$\phi = \phi_0 \quad (2)$$

Boundary Conditions ( $t > 0$ ) :

$$\frac{\partial \phi}{\partial \theta} = 0, \text{ at } \theta = 0 \text{ and } \pi \text{ (Symmetry Conditions)} \quad (3)$$

$$\phi = \phi_p, \text{ at } r = R \quad (4)$$

and as  $r \rightarrow \infty$ ,

Table 1 Source terms  $S_\phi$  in equation (1)

| $\phi$     | $\Gamma_\phi$ | $S_\phi$   |
|------------|---------------|--|
| $u_r$      | $\mu$         | $\frac{1}{r} \frac{\partial P}{\partial r} + \frac{1}{r^2} \frac{\partial}{\partial r}(\mu r^2 \frac{\partial u_r}{\partial r}) + \frac{1}{r \sin \theta} \frac{\partial}{\partial \theta}(\mu \sin \theta \frac{\partial u_\theta}{\partial r})$<br>$-\frac{1}{r^2 \sin \theta} \frac{\partial}{\partial \theta}(\mu \sin \theta u_\theta) - \frac{2u_r}{r^2} \frac{\partial u_\theta}{\partial \theta} - 4\mu \frac{u_r}{r^2}$<br>$-2\mu \frac{u_\theta \cot \theta}{r^2} + \rho \frac{u_\theta}{r^2}$   |
| $u_\theta$ | $\mu$         | $-\frac{\partial P}{\partial \theta} + \frac{1}{r^2} \frac{\partial}{\partial r}(\mu r^2 \frac{\partial u_\theta}{\partial r}) + \frac{1}{r^2 \sin \theta} \frac{\partial}{\partial \theta}(\mu \sin \theta \frac{\partial u_\theta}{\partial \theta})$<br>$+\frac{2}{r \sin \theta} \frac{\partial}{\partial \theta}(\mu \sin \theta \frac{u_r}{r}) + \frac{u_r}{r} \frac{\partial u_r}{\partial \theta} - \mu \frac{u_\theta}{r^2}$<br>$-2\mu \frac{u_r \cot \theta}{r^2} - 2\mu \frac{u_\theta \cot^2 \theta}{r^2} - \frac{1}{r^2} \frac{\partial}{\partial r}(\mu r u_\theta) - \rho \frac{u_r u_\theta}{r^2}$ |
| $i$        | $k/c_p$       | 0  |

$$\begin{aligned} u_\theta &= -(U_0 + U_1 \cos 2\pi ft) \sin \theta \\ u_r &= (U_0 + U_1 \cos 2\pi ft) \cos \theta \\ i &= i_\infty \end{aligned} \quad (5)$$

In Eqs. (4) and (5),  $\phi_p$  represents the value of the dependent variable  $\phi$  at the particle surface,  $U_0$  is the steady component of the flow velocity with respect to the particles and  $U_1$  is the peak value of the acoustic velocity. The velocities  $u_{rp}$  and  $u_{\theta p}$  in Eq. (4) are zero. The static enthalpy  $i_p$  is a constant value determined by a specified particle temperature.

In the presence of oscillating flow fields, the particle is at least partially entrained (but with a phase lag) in oscillating flow field. At high frequency, the magnitude of this entrainment is small. However, at low frequency, the particle is substantially entrained in the surrounding gas fields. In the present calculations, the particle momentum equation is included in order to consider particle entrainment.

The particle momentum equation is expressed as (Koopmann et al., 1989):

$$m_p \frac{dv_p}{dt} = \Gamma_d (v_g - v_p) \quad (6)$$

where

$$\Gamma_d = A_p \rho C_d |v_g - v_p| / 2 \quad (7)$$

$$C_d = (24 / Re) (1 + 0.15 Re^{0.687}) \quad (8)$$

$$A_p = 4\pi R^2 \quad (9)$$

where  $v_p$  in Eq. (6) represents the particle velocity and  $v_g$  represents  $U_0 + U_1 \cos 2\pi ft$  for the oscillating flow due to the acoustic field with a steady velocity component.

### 3. METHOD OF SOLUTION

The particle momentum conservation Eq. (6) with an unknown  $v_p$  are coupled to the gas phase conservation Eq. (1) with four unknowns ( $u_r, u_\theta, p, i$ ). Thus, coupled, nonlinear, unsteady and two-dimensional conservation equations with a total of five unknowns need to be solved simultaneously.

If the coordinate system is fixed in the ground, the grid system in the solution domain should move with the particle in order to consider particle entrainment. This is very difficult to implement numerically. In order to solve this problem, the coordinate system is fixed on the entrained particle. This results in the following extra source terms for the  $u_\theta$  and  $u_r$  since the coordinate system is noninertial:

$$S_{u_\theta} = S_{u_\theta} + \rho \frac{dv_p}{dt} \sin \theta \quad (10)$$

$$S_{u_r} = S_{u_r} - \rho \frac{dv_p}{dt} \cos \theta \quad (11)$$

The boundary conditions for  $u_\theta$  and  $u_r$  as  $r \rightarrow \infty$  are also adjusted as follows:

$$u_\theta = -(U_0 + U_1 \cos 2\pi ft - v_p) \sin \theta \quad (12)$$

$$u_r = (U_0 + U_1 \cos 2\pi ft - v_p) \cos \theta \quad (13)$$

The gas phase equations are first solved using the same SIMPLEC procedure of Doormaal and Raithby (1982). Using this solution, the particle conservation equations are solved

to yield the updated source terms for the gas phase, since the particle is entrained in the surrounding gas fields. The gas phase equations are solved again using these updated source terms, establishing the new solution for the gas field. This iterative procedure is repeated until the convergence criteria  $\epsilon_\phi$  for the gas phase equations given by Eq. (14) are satisfied.

$$\epsilon_\phi = \sum \left| \frac{\phi_{new} - \phi_{old}}{\phi_{new}} \right| \quad (14)$$

where  $\phi_{old}$  represents the values of the previous iteration and  $\phi_{new}$  the updated values from the present iteration for  $u_r, u_\theta$  and  $i$ .

The numerical solutions of the gas phase Eq. (1) and particle momentum Eq. (6) give the velocity and temperature fields for oscillating flow over a spherical particle as a function of time, with a particle velocity history. From the calculated temperature distribution, the local Nusselt number,  $Nu_\theta$ , is calculated as

$$Nu_\theta = \frac{h_\theta D}{k} = \frac{D}{(T_p - T_\infty)} \left. \frac{\partial T}{\partial r} \right|_{r=R} \quad (15)$$

Integrating the local Nusselt number in the axial direction, the space-averaged Nusselt number,  $Nu_s$ , is obtained. This is given by the following equation:

$$Nu_s = \frac{1}{\pi} \int_0^\pi Nu_\theta d\theta \quad (16)$$

## 4. RESULTS AND DISCUSSION

In the present simulation of heat transfer to and from a single spherical particle, the fluid is air with a free stream temperature of 20°C. The particle temperature is taken to be 40°C. The thermophysical properties such as viscosity, thermal conductivity, specific heat, etc. are calculated at a film temperature of 30°C since the property variation is small for the small temperature variation between 20°C and 40°C. The particle diameter is fixed at 100 μm in order to consider heat and mass transfer to and from small spherical particles such as pulverized coal particles and coal water slurry droplets. The numerical solution domain is chosen to be 20 times the particle diameter with 30 grid points in the  $\theta$ , and 50 in the  $r$  direction. The steady velocity ( $U_0$ ), the amplitude of the oscillating velocity ( $U_1$ ) and the frequency ( $f$ ) of the applied acoustic field are varied in order to obtain the values of the Nusselt numbers for different steady and acoustic Reynolds and Strouhal numbers. One period or cycle is divided into 40 uniform time intervals, so that  $\delta t = 1/40f$  is used as a numerical time step. A value of 0.005 is used for  $\epsilon_\phi$  in Eq. (14) as a convergence criterion in the present simulation.

Figure 2 shows a comparison of the separation angle  $\beta_s$  (measured in degrees) from the front stagnation point, obtained from the present simulation, with the approximate correlation given by Clift, Grace and Weber (1978), obtained from the numerical and experimental results for the steady Reynolds number range of 10 to 400 (without a superposed oscillating velocity,  $Re_1 = 0$ ). As shown in Fig. 2, the present results for the separation angle  $\beta_s$  represent well the correlation given by Clift, Grace and Weber (1978). Figure 2 also shows a comparison of the Nusselt number obtained from the present simulation with previously published numerical and

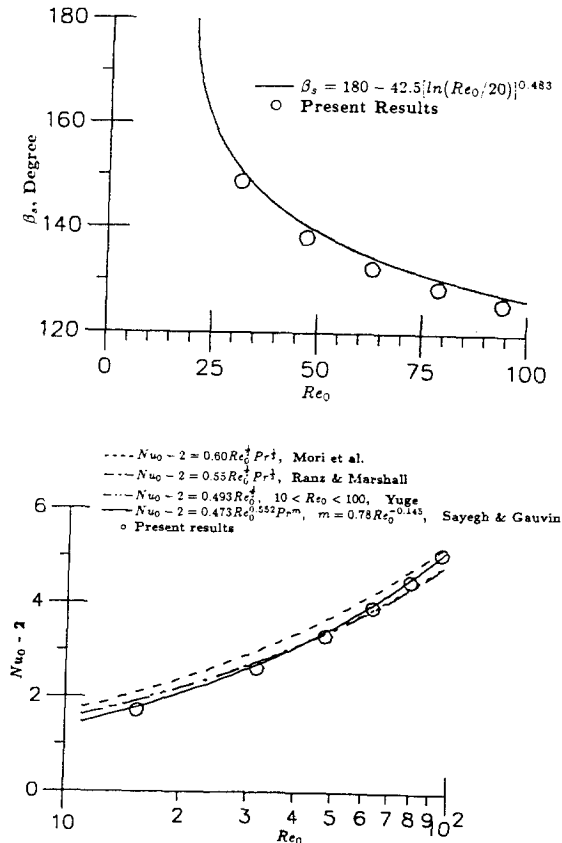


Fig. 2 Comparisons of separation angle ( $\beta_s$ ) and Nusselt number ( $Nu_0-2$ ) obtained from the present simulation, with previous numerical and experimental results

experimental results by Ranz and Marshall (1952), Yuge (1960), Mori et al. (1969) and Sayegh and Gauvin (1979) for the steady Reynolds number range of 10 to 100 (without a superposed oscillating velocity,  $Re_1=0$ ). The present results agree well with the numerical results given by Sayegh and Gauvin (1979). Sayegh and Gauvin (1979) indicated excellent agreement between previous numerical results and their calculations. They used a  $30 \times 40$  grid in the  $\theta$  and  $r$  directions, respectively. However, the present results are somewhat higher than Yuge's correlation (1960) obtained from experimental data for Reynolds numbers around 100 and are somewhat lower for Reynolds numbers around 10. This is also true for the numerical results of Sayegh and Gauvin (1979) and Wong, Lee and Chen (1986). For the case of an oscillating flow with and without a steady velocity component under the assumption that the particle is not entrained but is stationary in the presence of an oscillating flow, the results for space and time-averaged Nusselt number using a present code represent well the correlations obtained from the quasi-steady analysis for a frequency of 50 Hz, as shown by Ha (1991). Under the assumptions of no particle entrainment, the particle momentum Eq. (6) is not considered ( $v_p=0$ ). These comparisons show that the present code is adequate for predicting the steady and oscillating flow field and heat transfer for a spherical particle.

#### 4.1 Oscillating Flow With a Steady Velocity

Figure.3 shows the oscillating flow  $U(=U_0+U_1\cos 2\pi ft)$ , the

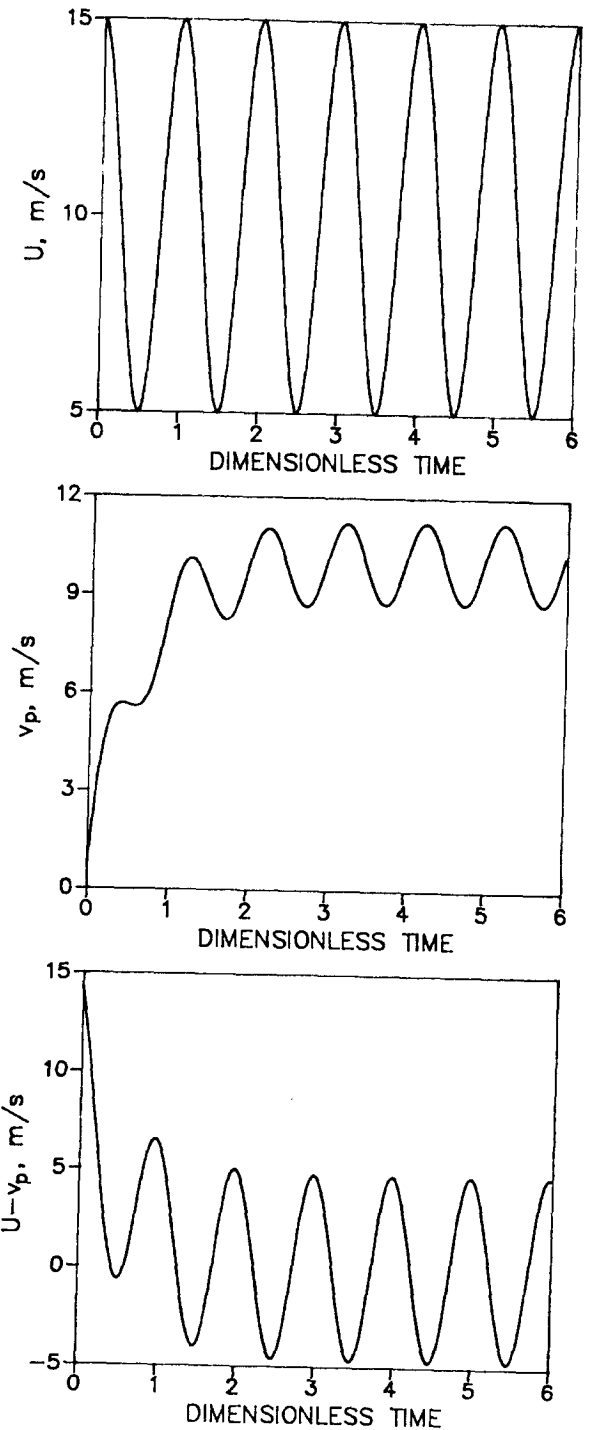


Fig. 3 Oscillating flow  $U$ , the entrained particle velocity  $v_p$  and the relative velocity ( $U-v_p$ ) as a function of dimensionless time;  $Re_0=62.9$ ,  $Re_1=31.5$ ,  $S=0.00005$  ( $f=50\text{Hz}$ )

entrained particle velocity  $v_p$  and the relative velocity ( $U-v_p$ ) at 50 Hz, in order to investigate heat transfer past particles entrained in an oscillating flow with a steady velocity component. The applied acoustic field  $U$  oscillates with an amplitude of 5m/s around a steady velocity of 10m/s. During the initial and transient period, the particle velocity increases to about 10m/s due to a major contribution of a steady velocity  $U_0$ , meaning that the particle is almost

entrained to the steady flow. After a quasi-steady state is reached, meaning that the particle velocity over a cycle is the same as the value obtained in the following cycles, the particle velocity oscillates with an amplitude of about 1.24m/s around a steady velocity of 10m/s. The phase lag between the gas and particle velocity is about  $78^\circ$  ( $\tau=0.2$ ). Thus the relative velocity ( $U-v_p$ ) has an initial decrease due to particle entrainment to the steady flow, followed by the quasi-steady oscillation with an amplitude of about 4.7m/s, as shown in Fig. 3. The phase lag between the gas and relative velocity is about  $18^\circ$  ( $\tau=0.05$ ). Even though the particle oscillates with an amplitude of 1.24m/s around a steady velocity, the amplitude of relative velocity still has a value of 4.7m/s slightly lower than the oscillating velocity  $U_1$  ( $=5$  m/s), due to the phase difference. Thus, the boundary layer formed over the particles is reversed with every half-period of an oscillating flow. However, for stationary particles exposed to an oscillating flow with and without a steady velocity as shown in experimental works (Mori et al., 1969, Gibert and Angelino, 1974, Larsen and Jensen, 1978) and theoretical works (Ha, 1991), the particle velocity is zero and the relative velocity is the same as an oscillating flow. Thus the relative velocity with no particle entrainment oscillates with an amplitude of 5m/s around a steady velocity of 10m/s and the flow direction is always from left to right, unlike the case with particle entrainment having a flow direction reversing every half-period. These results show that the heat

transfer past particles with entrainment has different characteristics compared with that without entrainment.

Figure 4 shows the local Nusselt number variation with angle for  $Re_0=62.9$  and  $Re_1=31.5$  at a frequency of 50 Hz. The local Nusselt numbers with particle entrainment are compared with the quasi-steady, local Nusselt number without particle entrainment. The Nusselt number is plotted as  $Nu_\theta-2$  to separate effects of pure conduction from convection.  $Nu_\theta=2$  corresponds to a pure conduction value.  $Nu_\theta-2$  with entrainment decreases with increasing particle velocity due to the particle entrainment (see Fig. 3), followed by the quasi-steady state after about four cycles. The relative velocities with entrainment at  $\tau=0.0, 1.0, 2.0, 3.0, 4.0$  and  $5.0$  are 15, 6.24, 4.88, 4.64, 4.59 and 4.58m/s, respectively, resulting in the decreasing  $Nu_\theta-2$  with decreasing relative velocity due to particle entrainment, as shown in Fig. 4. However, the relative velocity without entrainment is 15 m/s, giving  $Nu_\theta-2$  varying in the range of 0.7~10.64, larger than  $Nu_\theta-2$  with entrainment varying in the range of 0.1~5.1 at  $\tau=5.0$ . At these dimensionless times, the flow direction at infinity is from left to right both with and without particle entrainment, in the coordinate system as shown in Fig. 1. Thus  $Nu_\theta-2$  has a maximum value at the stagnation point at  $\theta=180$  and decreases along the stream-wise direction ( $\theta=180 \rightarrow \theta=0$ ). In the following dimensionless times of  $\tau=0.25, 1.25, 2.25, 3.25, 4.25$  and  $5.25$ , the relative velocities with entrainment are 4.78,  $-0.095, -0.24, -1.15, -1.17$

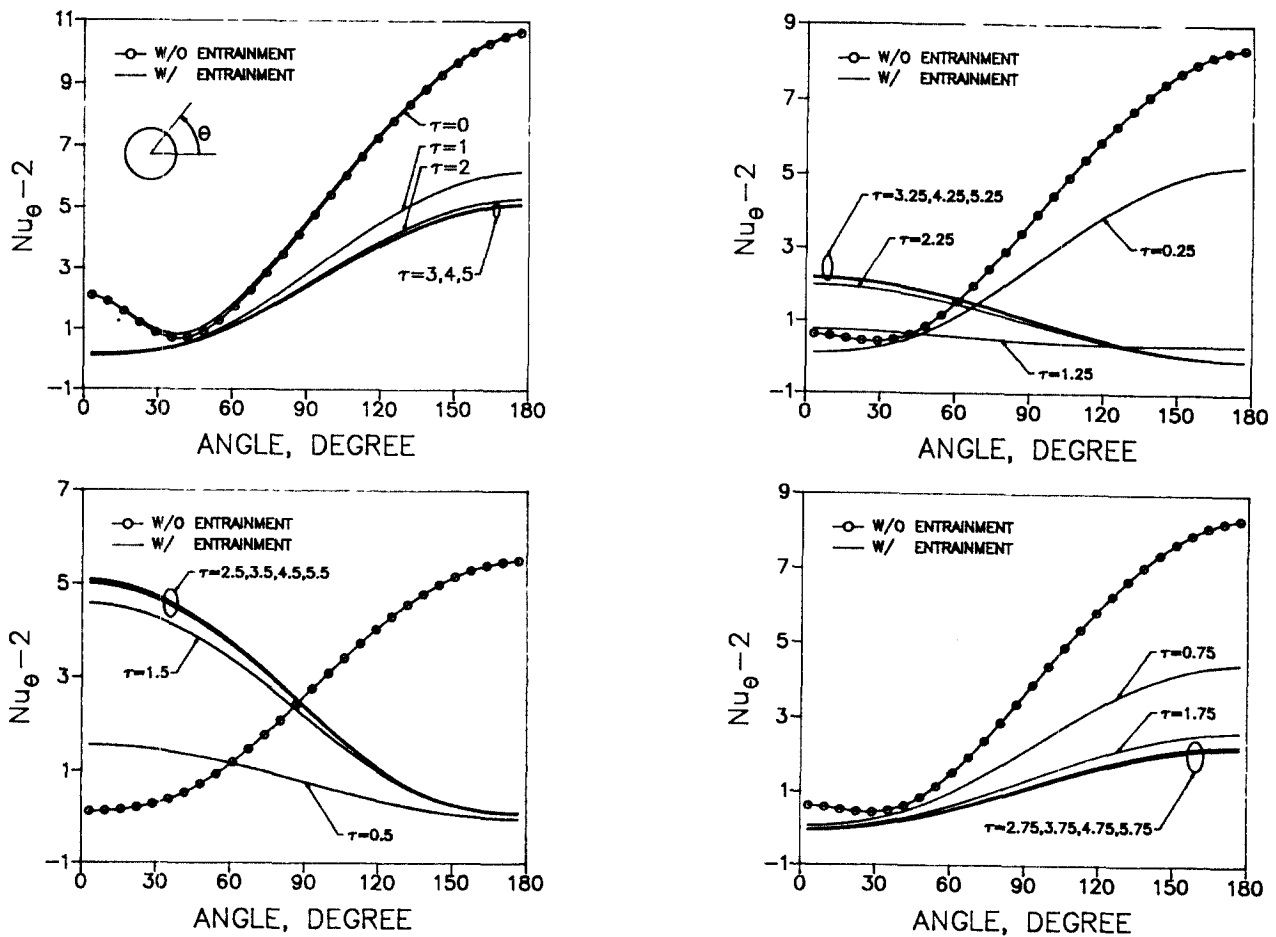


Fig. 4 Angular variation of local Nusselt number with and without particle entrainment:  $Re_0=62.9$ ,  $Re_1=31.5$ ,  $S=0.0005$  ( $f=50$ Hz)

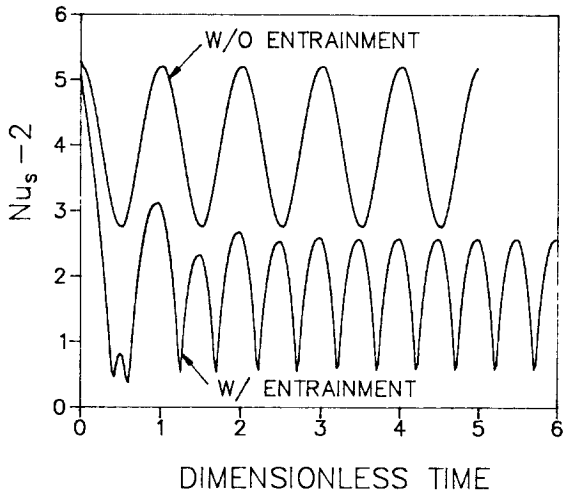


Fig. 5 Space-averaged Nusselt number with and without particle entrainment as a function of dimensionless time:  $Re_0 = 62.9$ ,  $Re_1 = 31.5$ ,  $S = 0.005$  ( $f = 50\text{Hz}$ )

and  $-1.18\text{m/s}$ . Thus the flow direction at  $\tau = 0.25$  is from left to right with a stagnation point at  $\theta = 180$ . But the flow direction at  $\tau = 1.25, 2.25, 3.25, 4.25$  and  $5.25$  is reversed to that from right to left with a stagnation point at  $\theta = 0$  due to the particle entrainment. The relative velocity without entrainment is  $10\text{m/s}$  with a stagnation point at  $\theta = 180$  with a flow direction from left to right, giving  $Nu_\theta - 2$  varying in the range of  $0.04 \sim 8.4$ , larger than  $Nu_\theta - 2$  with entrainment varying in the range of  $-0.006 \sim 2.2$  at  $\tau = 5.25$ . At  $\tau = 0.5, 1.5, 2.5, 3.5, 4.5$  and  $5.5$ , the relative velocities with entrainment increases from  $-0.62$  to  $-4.58\text{m/s}$  with a flow direction from right to left. The relative velocity without entrainment is  $5\text{m/s}$  with a flow direction from left to right, slightly larger than  $-4.58\text{m/s}$  with entrainment at  $\tau = 5.5$ . Thus  $Nu_\theta - 2$  with entrainment at  $\tau = 5.5$  has a symmetric profile around  $\theta = 90$ , compared to that without entrainment. The relative velocities at  $\tau = 0.75, 1.75, 2.75, 3.75, 4.75$  and  $5.75$  decreases from  $3.85$  to  $1.18\text{m/s}$  with increasing particle velocity due to particle entrainment. These relative velocities with entrainment are smaller than  $10\text{m/s}$  without entrainment, resulting in the lower  $Nu_\theta - 2$  with entrainment compared with that without entrainment.

Figure 5 shows the space-averaged Nusselt number ( $Nu_s - 2$ ) with and without particle entrainment as a function of dimensionless time  $\tau$  for the oscillating flow with steady Reynolds number  $Re_0 = 62.9$  and acoustic Reynolds number  $Re_1 = 31.5$  for Strouhal number of  $0.001$ . The space-averaged Nusselt number  $Nu_s$  is calculated from  $Nu_\theta$  using Eq. (16). As shown in Fig. 5,  $Nu_s - 2$  without entrainment shows the same cyclic behavior as the sinusoidal relative velocity (same as the oscillating velocity with a steady velocity). However, for  $Nu_s - 2$  with entrainment, another high peak at the half time of the period in each cycle is observed. This happens since the space-averaged Nusselt number is not dependent on the direction of the velocity, which changes as a result of the acoustic field, and is dependent only on the magnitude of the total flow velocity.

Figure 6 shows the oscillating flow  $U$ , the entrained particle velocity  $v_p$  and the relative velocity ( $U - v_p$ ) at  $2000\text{Hz}$ , in order to investigate the frequency effect on the heat transfer past particles entrained in an oscillating flow with a steady

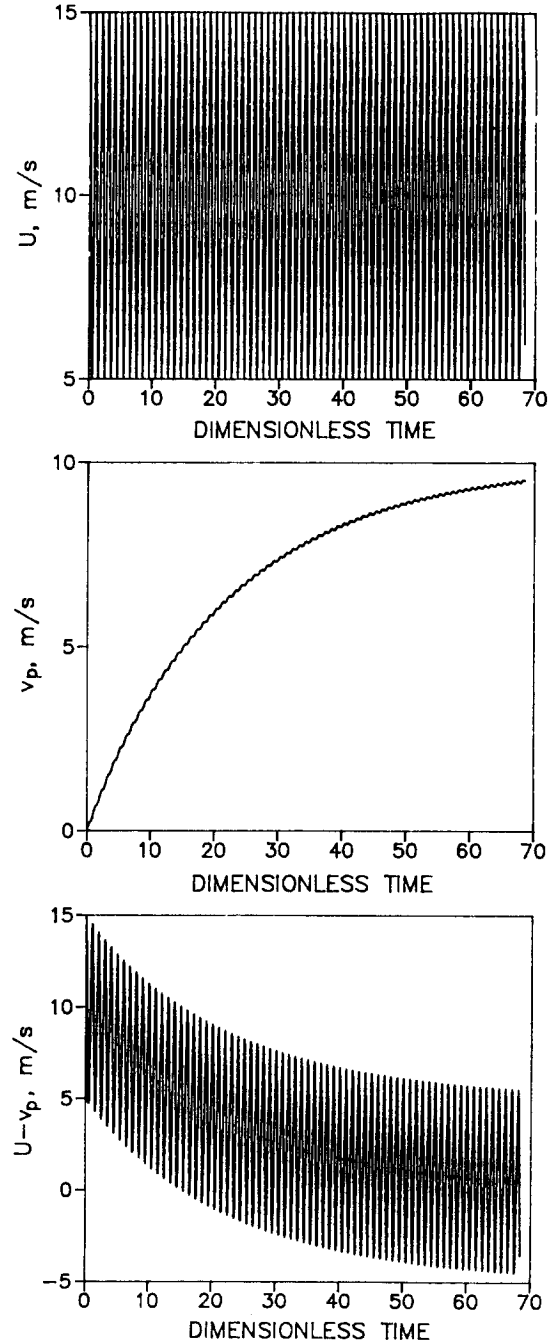


Fig. 6 Oscillating flow  $U$ , the entrained particle velocity  $v_p$  and the relative velocity ( $U - v_p$ ) as a function of dimensionless time:  $Re_0 = 62.9$ ,  $Re_1 = 31.5$ ,  $S = 0.02$  ( $f = 2000\text{Hz}$ )

velocity component. Similar to the case of  $f = 50\text{Hz}$ , the applied acoustic field  $U$  oscillates with an amplitude of  $5\text{m/s}$  around a steady velocity of  $10\text{m/s}$ , giving  $Re_0 = 62.9$ ,  $Re_1 = 31.5$  and  $S = 0.02$ . As shown in Fig. 3, it takes more than three cycles in order for the relative velocity at  $f = 50\text{Hz}$  to reach a quasi-steady state after the particle is almost entrained in the steady velocity  $U_0$ . Three cycles at  $50\text{Hz}$  corresponds to 120 cycles for  $2000\text{Hz}$ . Thus the results up to around 70 cycles are shown in the present calculation for  $f = 2000\text{Hz}$  due to severe computational time. The entrained particle velocity approaches the steady velocity  $U_0 (= 10\text{m/s})$ .

After the initial and transient period, the relative velocity is expected to approach the oscillating flow with an amplitude of 5m/s which is the acoustic velocity  $U_1 \cos 2\pi ft$ , as shown in Fig. 6. Thus the space-averaged Nusselt number ( $Nu_s-2$ ) with entrainment has different time histories compared with  $Nu_s-2$  without entrainment, as shown in Fig. 7.  $Nu_s-2$  without entrainment reaches a quasi-steady state at an early cycle and oscillates in the range of 2.8~5.1. However the value of  $Nu_s-2$  with entrainment decreases during the initial and transient period until it reaches a quasi-steady state.  $Nu_s-2$  with entrainment is lower than that without entrainment due to particle entrainment.

### 4.2 Oscillating Flow Without a Steady Velocity

Figure.8 shows the oscillating flow  $U$ , the entrained particle velocity  $v_p$  and the relative velocity ( $U-v_p$ ) at 50 Hz, in order to investigate heat transfer past particles entrained in an oscillating flow without a steady velocity component. The applied acoustic field  $U$  oscillates with an amplitude of 10m/s, giving acoustic Reynolds number of 62.9 and Strouhal number of 0.0005. For this small value of the Strouhal number, the velocity and temperature field reaches a quasi-steady state after an early cycle. Thus the following discussion

concentrates on the results over one cycle after reaching a quasi-steady state, unless it is mentioned otherwise. While the oscillating flow  $U$  oscillates with an amplitude of 10m/s, the particle velocity  $v_p$  oscillates with an amplitude of 2.72m/s with a phase lag of about  $72^\circ$  ( $\tau=0.2$ ). Due to this phase lag between an oscillating flow and particle velocity, the relative velocity,  $U-v_p$ , oscillates with an amplitude of 9.38m/s slightly lower than an oscillating flow  $U$  which is the relative velocity without entrainment. The phase lag between an oscillating flow,  $U$ , and the relative velocity,  $U-v_p$ , is about

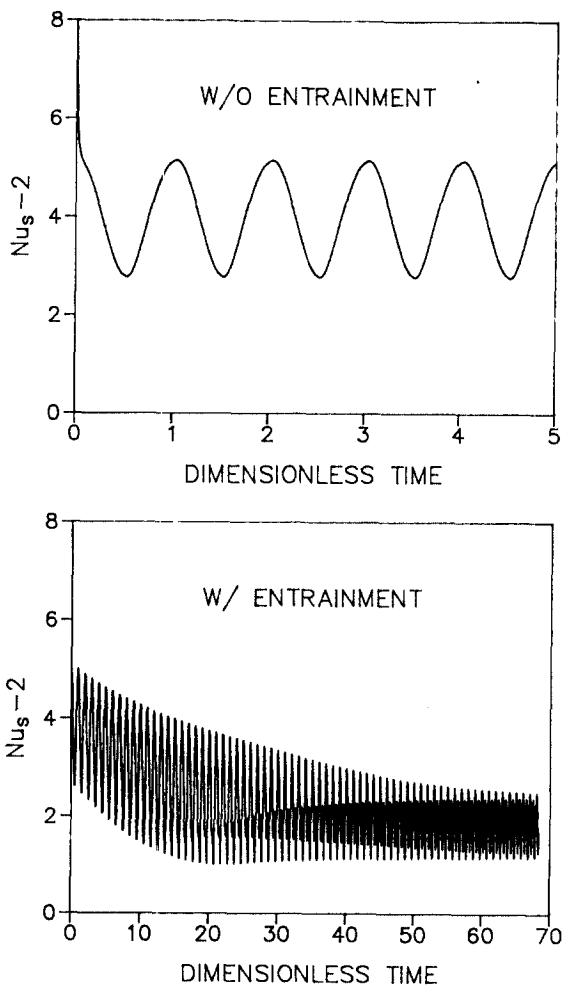


Fig. 7 Space-averaged Nusselt number with and without particle entrainment as a function of dimensionless time:  $Re_0 = 62.9$ ,  $Re_1 = 31.5$ ,  $S = 0.02$  ( $f = 2000\text{Hz}$ )

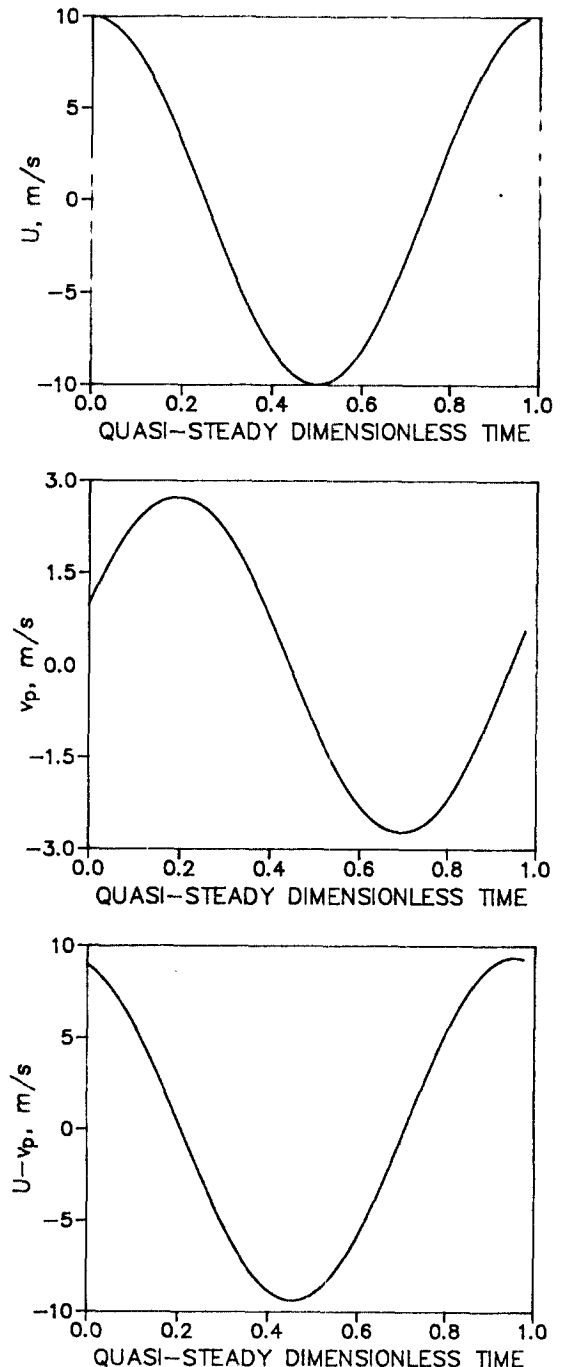


Fig. 8 Oscillating flow  $U$ , the entrained particle velocity ( $U-v_p$ ) as a function of quasi-steady dimensionless time:  $Re_0 = 0$ ,  $Re_1 = 62.9$ ,  $S = 0.0005$  ( $f = 50\text{Hz}$ )

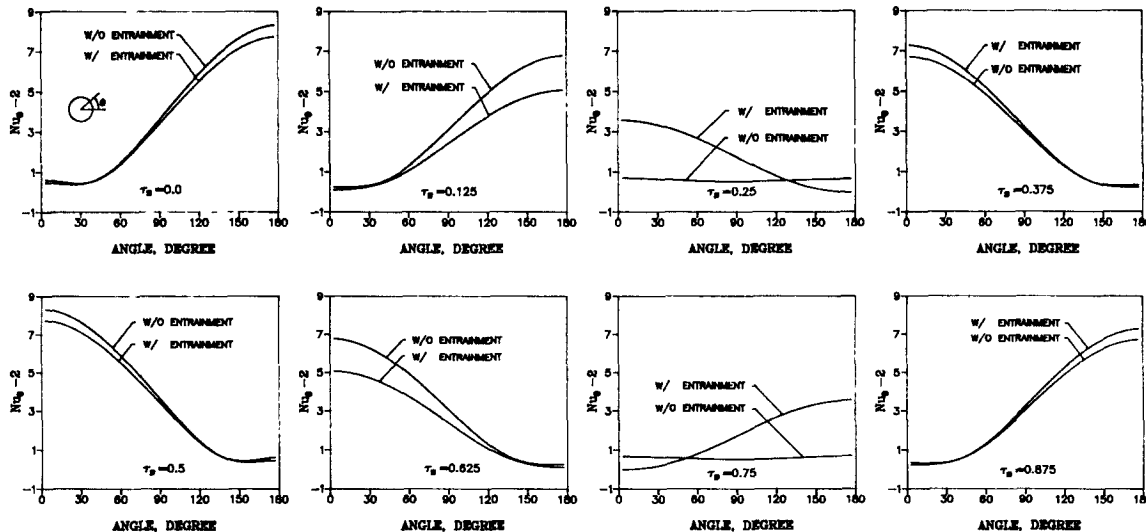


Fig. 9 Angular variation of local Nusselt number with and without particle entrainment :  $Re_0=0, Re_1=62.9, S=0.0005 (f=50\text{Hz})$

$18^\circ (\tau=0.05)$ .

Figure.9 shows the quasi-steady, local Nusselt number variation with angle without steady flow corresponding to  $Re_1=62.9$  and  $S=0.005$ . The results with entrainment are compared with that without entrainment. At  $\tau=0.0$ , the oscillating velocity is 10m/s and the particle velocity is 1 m/s. Thus the relative velocity with entrainment is 9m/s, lower than 10m/s without entrainment.  $Nu_{\theta-2}$  with entrainment is lower than that without entrainment, due to the difference in the relative velocity with and without entrainment. The difference in  $Nu_{\theta-2}$  at the stagnation point ( $\theta=180$ ) is about 7%. In the following dimensionless time  $\tau=0.125$ , the particle velocity is 2.5m/s for the oscillating velocity of 7.07m/s. Thus the relative velocity with entrainment is 4.57m/s which is 54% lower than the relative velocity without entrainment.  $Nu_{\theta-2}$  with entrainment at the stagnation point ( $\theta=180$ ) is about 25% lower than that without entrainment. At  $\tau=0.25$ , the relative velocity without entrainment is 0 m/s which is the same as the oscillating velocity. As shown in Andres and Ingard (1953a) and Andres and Ingard (1953b), a small steady motion (acoustic streaming) is generated over a spherical particle in the presence of an acoustic field. Thus, as shown by Ha(1991), it is expected that the phase lag between the applied acoustic field and the thermal boundary layer, and the steady streaming results in  $Nu_{\theta-2}$  without entrainment varying in the range of 0.5~0.7, even though the relative velocity is 0 m/s.

However, for the case with entrainment, the relative velocity is -2.5m/s with a stagnation point at  $\theta=0$ . Thus  $Nu_{\theta-2}$  with entrainment varies in the range of -0.001~3.6, larger than  $Nu_{\theta-2}$  without entrainment. In the following dimensionless time  $\tau=0.375$ , the relative velocity without entrainment is -7.07m/s which is the same magnitude as that at  $\tau=0.125$  with a flow direction from right to left. Thus  $Nu_{\theta-2}$  without entrainment at  $\tau=0.375$  has a symmetric profile around  $\theta=90$ , compared to  $Nu_{\theta-2}$  without entrainment at  $\tau=0.125$ . The relative velocity with entrainment at  $\tau=0.375$  is -8.2m/s with a flow direction from right to left. This relative velocity with entrainment at  $\tau=0.375$ m/s is about 80% larger than the relative velocity with entrainment at  $\tau=0.125$  and about 17% larger than the relative velocity without

entrainment at  $\tau=0.375$ . This results in the larger  $Nu_{\theta-2}$  with entrainment at  $\tau=0.375$ , compared to that with entrainment at  $\tau=0.125$  and that without entrainment at  $\tau=0.375$ . The differences in the maximum  $Nu_{\theta-2}$  at the stagnation point with entrainment at  $\tau=0.375$  are 8.4 and 43%, respectively, compared with that without entrainment at  $\tau=0.375$  and that with entrainment at  $\tau=0.125$ . At  $\tau=0.5$  the oscillating velocity and the relative velocity without entrainment have a peak value of -10m/s. The relative velocity with entrainment at  $\tau=0.5$  is 9m/s which is the same magnitude as the relative velocity with entrainment at  $\tau=0.0$  and 10% lower than the relative velocity without entrainment at  $\tau=0.5$ .  $Nu_{\theta-2}$  with entrainment at  $\tau=0.5$  has a symmetric shape around  $\theta=90$ , compared with  $Nu_{\theta-2}$  with entrainment at  $\tau=0$ , and is lower than  $Nu_{\theta-2}$  without entrainment at  $\tau=0.5$  with 7.5% difference at a stagnation point. The distribution of  $Nu_{\theta-2}$  with and without particle entrainment at a dimensionless time from  $\tau=0.5$  to 0.75 is very similar to that from  $\tau=0.0$  to 0.25, and that at a dimensionless time from  $\tau=0.75$  to 1.0 is very similar to that from  $\tau=0.25$  and 0.75 except that they are

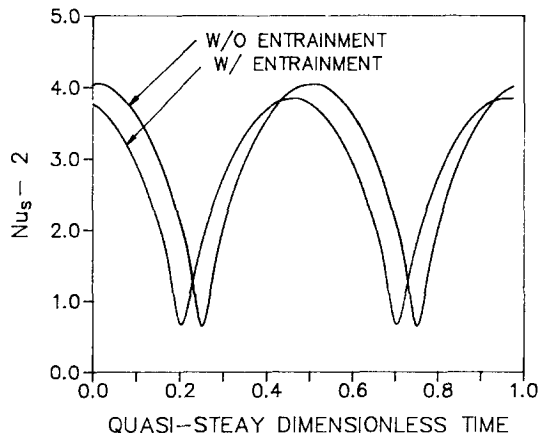


Fig. 10 Space-averaged Nusselt number with and without particle entrainment as a function of quasi-steady dimensionless time :  $Re_0=0, Re_1=62.9, S=0.0005 (f=50\text{Hz})$



anti-symmetric.

The space-averaged Nusselt number with and without particle entrainment is shown in Fig. 10 for  $Re_1=62.9$  and  $Re_0=0.0$  for  $S=0.0005$  ( $f=50\text{Hz}$ ) as a function of dimensionless time.  $Nu_s-2$  with and without entrainment has two high and low peak values over one cycle corresponding to the maximum and minimum values of the relative velocity with and without entrainment, respectively.  $Nu_s-2$  with entrainment varies in the range of  $0.68\sim 3.84$  over one cycle after the quasi-steady state has been reached, whereas  $Nu_s-2$  without

entrainment is in the range of  $0.65\sim 4.04$ , due to about 6% difference in the relative velocity with and without entrainment. The phase lag between the space-averaged Nusselt number with and without entrainment is about  $18^\circ$ .

Figure.11 shows the oscillating flow  $U$ , the entrained particle velocity  $v_p$  and the relative velocity ( $U-v_p$ ) for  $Re_1=62.9$  and  $S=0.02$  ( $f=2000\text{Hz}$ ). The particle velocity oscillates with an amplitude of about  $0.07\text{m/s}$  with  $81^\circ$  phase lag ( $\tau=0.225$ ) between  $U$  and  $v_p$ . Since the particle velocity with particle entrainment oscillates with very small amplitude, the relative velocity with entrainment is almost the same as the oscillating flow velocity  $U$  which is the relative velocity without entrainment. Thus the local and space-averaged Nusselt number with particle entrainment is almost the same as that without particle entrainment. Since the results for the local and space-averaged Nusselt number without particle entrainment at  $f=2000\text{Hz}$  have been shown in details by Ha (1991), the discussion about these results are not shown in the present paper.

## 5. SUMMARY AND CONCLUSIONS

The axisymmetric and laminar conservation equations for mass, momentum and energy are solved numerically in order to investigate the effects of particle entrainment on the heat transfer past a single spherical particle entrained in an oscillating flow with and without a steady velocity component. The results with particle entrainment are compared with the case without particle entrainment. The followings are the major findings of the present studies.

The moving particle in the presence of an oscillating flow with a steady velocity is entrained in the steady velocity  $U_0$  and the relative velocity close to the oscillating velocity  $U_1 \cos 2\pi ft$  can be used for heat transfer past particles. However, for the stationary particles fixed in the atmosphere, the sum of oscillating and steady velocity is used for heat transfer past particles. This results in the lower space-averaged Nusselt number with particle entrainment compared with that without particle entrainment, corresponding to almost the steady velocity.

In the presence of the oscillating flow, the magnitude of particle entrainment decreases and the phase lag between the particle movement and the oscillating flow increases with increasing frequency. At  $50\text{ Hz}$ , the particle is entrained in the oscillating flow with a phase lag. Due to this phase lag, the relative velocity between the flow and the particle has an amplitude slightly lower than that of oscillating flow  $U$ , giving slightly lower space-averaged Nusselt number with entrainment compared with the case without entrainment. The difference in the maximum value of  $Nu_s-2$  with and without particle entrainment is about  $5.2\%$  for  $Re_0=0$ ,  $Re_1=62.9$  and  $S=0.0005$  ( $f=50\text{Hz}$ ) and the phase lag between  $Nu_s-2$  with and without entrainment is about  $18^\circ$ . If the frequency is increased to  $2000\text{ Hz}$ , the particle entrainment is very small and the relative velocity with and without particle entrainment is almost the same, resulting in the same space-averaged Nusselt number with and without particle entrainment.

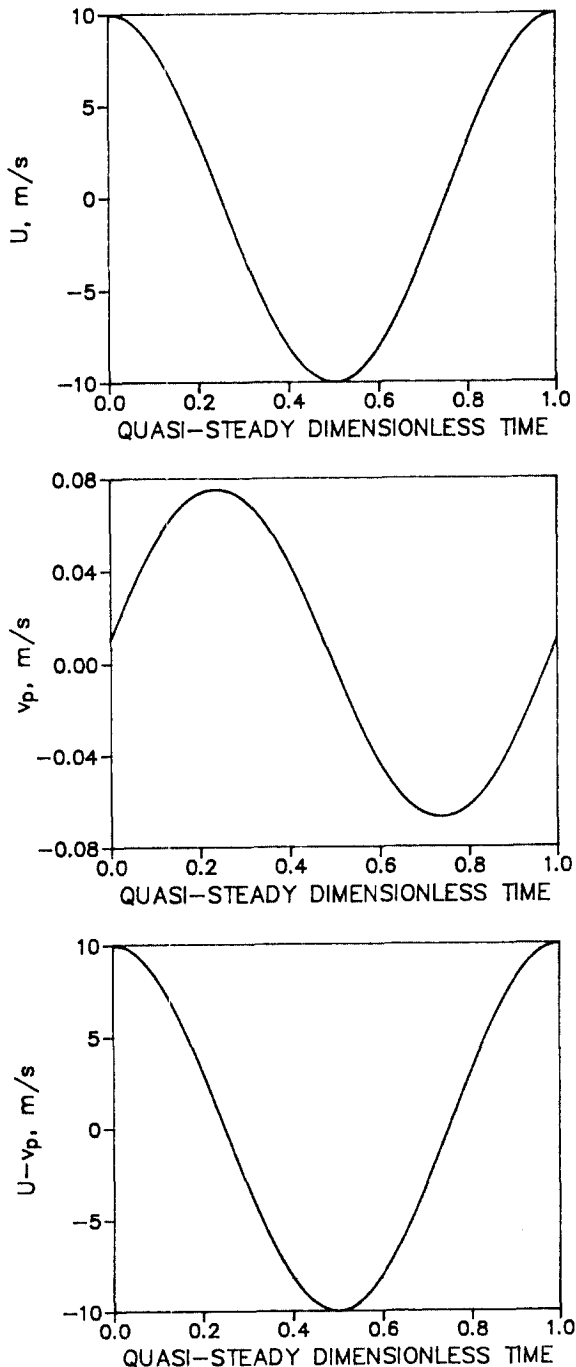


Fig. 11 Oscillating flow  $U$ , the entrained particle velocity  $v_p$  and the relative velocity ( $U-v_p$ ) as a function of quasi-steady dimensionless time:  $Re_0=0$ ,  $Re_1=62.9$ ,  $S=0.02$  ( $f=2000\text{ Hz}$ )

## REFERENCES

Andres, J.M. and Ingard, U., 1953a, "Acoustic Streaming at

High Reynolds Number," *The Journal of the Acoustical Society of America*, Vol. 25, No. 5, pp. 928~932.

Andres, J.M. and Ingard, U., 1953b, "Acoustic Streaming at Low Reynolds Number," *The Journal of the Acoustical Society of America*, Vol. 25, No. 5, pp. 932~938.

Baxi, C.B. and Ramachandran, A., 1969, "Effect of Vibration on Heat Transfer from Spheres," *Trans. ASME, J. of Heat Transfer*, pp. 337~344.

Clift, R., Grace, J.R. and Weber, M.E., 1978, "Bubbles, Drops, and Particles," Academic Press, Inc.

Doormaal, J.P. and Raithby, G.D., 1982, "Enhancement of the SIMPLE Method for Predicting Incompressible Fluid Flow," *Numerical Heat Transfer*, Vol. 7, pp. 147~163.

Faeser, R.J., 1984, "Acoustic Enhancement of Pulverized Coal Combustion," ASME Paper, 84-WA/NCA-18.

Gibert, H. and Angelino, 1974, "Transferts De Matiere Entre Une Sphere Soumise A Des Vibrations Et Un Liquide En Mouvement," *Intl. J. Heat and Mass Transfer*, Vol. 17, pp. 625~632.

Ha, M.Y., 1990, "A Theoretical Study of Augmentation of Particle Combustion Via Acoustic Enhancement of Heat and Mass Transfer," Ph.D. Thesis, The Pennsylvania State University.

Koopmann, G.M., Scaroni, A.W., Yavuzkurt, S., Reethof, G., Ramachandran, P. and Ha, M.Y., 1989, "Acoustically Enhanced Combustion of Micronized Coal Water Slurry Fuel," Final Report to DOE/METC under Contract No. DE-RA21-86MC23257.

Larsen, P.S. and Jensen, J.W., 1978, "Evaporation Rates of Drops in Forced Convection with Superposed Transverse Sound Field," *Intl. J. Heat and Mass Transfer*, Vol. 21, pp. 511~517.

Marthelli, R.C. and Boelter, L.M.K., 1939, "The Effect of Vibration on Heat Transfer by Free Convection from a Horizontal Cylinder," *Proc. 5th Intl. Congress of Applied Mechanics*, pp. 578~584.

Mori, Y., Imabayashi, M., Hijikata, K. and Yoshida, Y.,

1969, "Unsteady Heat and Mass Transfer from Spheres," *Intl. J. Heat Mass Transfer*, Vol. 12, pp. 571~585.

Patankar, S.V., 1980, "Numerical Heat Transfer and Fluid Flow," Hemisphere, Washington D.C.

Ranz, W.E. and Marshall, W.R., 1952, "Evaporation From Drops," *Chemical Engineering Progress*, Vol. 48, pp. 141~146.

Rawson, S.A., 1988, "An Experimental Investigation of the Influence of High Intensity Acoustics on Heat and Mass Transfer Rates from Spheres as Related to Coal-Water Slurry Fuel Combustion Enhancement," M.S. Thesis, The Pennsylvania State University.

Sayegh, N.N. and Gauvin, W.H., 1979, "Numerical Analysis of Variable Property Heat Transfer to a Single Sphere in High Temperature Surroundings," *AICHE J.*, Vol. 25, No. 3, pp. 522~534.

Yavuzkurt, S. and Ha, M.Y., Koopmann, G.M. and Scaroni, A. W., 1989, "A Model of the Enhancement of Coal Combustion Using High Intensity Acoustic Fields," 1989 National Heat Transfer Conference, HTD Vol. 106, Heat Transfer Phenomena in Radiation, Combustion and Fires, pp. 439~446, Aug. 6~9, Philadelphia.

Yavuzkurt, S. and Ha, M.Y., 1989, "A Model of the Enhancement of the Combustion of Coal Water Slurry Fuels Using High Intensity Acoustic Fields," 89 WA/NCA-2, ASME Winter Annual Meeting, Dec. 10~15, San Francisco.

Yuge, T., 1960, "Experiments on Heat Transfer From Spheres Including Combined Natural and Forced Convection," *J. of Heat Transfer, Trans. ASME, Series C.*, Vol. 82, pp. 214~220.

Zinn, B.T., Carvalho Jr., J.R., Miller, N. and Daniel, B.R., 1982, "Pulsating Combustion of Coal in a Rijke Type Combustor," 19th Symposium (Interantional) on Combustion, the Combustion Institute, pp. 1197~1203.

Wong, K, Lee, S. and Chen, C., 1986, "Finite Element Solution of Laminar Combined Convection From a Sphere," *J. of Heat Transfer*, Vol. 108, pp. 860~865